THE JOURNAL OF PHYSICAL CHEMISTRY C

pubs.acs.org/JPCC Article

Transport and Structure of Room-Temperature Ionic Liquids in Conical Nanopores under External Electric Fields

Xikai Jiang*

Cite This: J. Phys. Chem. C 2020, 124, 5817−5828 Read Online

ABSTRACT: The transport and structure of room-temperature ionic liquids (RTILs) in conical nanopores under external electric fields were studied using molecular dynamics simulations. Electrically neutral, nonuniformly charged, and uniformly charged nanopores were considered. The current−voltage relationship was calculated as the macroscopic transport property. When the magnitude of the applied voltage increases, the magnitude of the current was found to increase nonlinearly with an increasing slope. The nonlinearity was traced back to that the RTILs' electrical conductivity increases as the magnitude of the electric field increases and as the ion concentration decreases (ion depletion) because of the solvent-free nature of the RTILs. The degree of ion depletion is highest near the pore tip, and it decreases as the location moves from the tip to the base, because the electric field is strongest near the tip while RTILs are more bulk-like near the base and their conductivities' dependence on the electric field is weaker than that near the tip. At the same applied voltage, the current through the nonuniformly charged pore was weaker than that through the neutral pore, while the current through the uniformly charged pore was stronger. This is because the hindered transport due to the higher total ion concentration and the lower degree of ion depletion dominates in the nonuniform case, while the enhanced transport due to the formation of electrical double layers (EDLs) dominates in the uniform case. Cation and anion currents were calculated separately, and the results show that negatively charged nanopores are cation-selective. EDLs were observed near pore walls due to the external electric field and surface charges, and the results suggest that the ion density in EDLs is tunable by varying the applied voltage across the system. The physical insights provided in this study demonstrate the importance of solvent-free nature and strong ion−ion correlations in RTILs on their nonequilibrium transport and structures in nanopores, and the results imply that the charging dynamics of RTILs in nanoporous electrodes in supercapacitor and energy applications could be greatly enhanced under larger applied voltages.

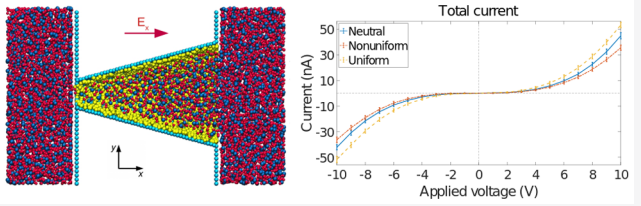

INTRODUCTION

Ionic transport through nanopores is a fundamental process underpinning a wide variety of applications. In electrical double layer (EDL) capacitors, accumulated charges on nanoporous electrodes attract counterions from the electrolyte to electrodes' surface, forming EDLs that store energy. Ionic transport through nanopores in electrodes determines the performance of EDL capacitors such as power density and the time for charging and discharging.[1−4] In salinity gradient power generators, the ionic concentration gradient drives ionic transport in ion-selective membranes, and the associated osmotic energy can be harvested directly in the form of electrical energy. Optimizing geometries and surface charge densities in the ion-selective membranes can enhance the power density of the generators.[5−7] In biology, ionic transport through lipid bilayers, specialized ion pumps, and protein channels in cell membranes are crucial to sustain cellular function.[8] Through decades of research on ionic transport in diverse systems and applications at nanoscales,[9] a wide variety of intriguing transport phenomena have been discovered and extensively studied. Examples include concentration polarization,[10−13] ion enrichment-depletion,[14−16] current rectification,[17−22] anomalous transport effects,[23−26] selective ion transport,[27−30] and memory effects,[31−33] just to name a few.

Studies on ionic transport through conical nanopores have drawn much attention in the past decade. Unique properties such as the symmetry-breaking geometry play important roles in ionic transport through conical nanopores and the associated transport phenomena such as the current rectification. Systematic studies have been performed using theories and experiments to probe the effect of surface charge and geometry on the current rectification in conical nanopores.[34−38] In theoretical works,[34,35] the author divided the pore into a region near the tip, a region near the base, and a transition region, and the different transference numbers in different regions lead to the

Received: October 30, 2019
Revised: February 20, 2020
Published: February 21, 2020

https://dx.doi.org/10.1021/acs.jpcc.9b10201
J. Phys. Chem. C 2020, 124, 5817−5828

rectification in this model. For numerical studies, the one-dimensional (1D) Poisson−Nernst−Planck (PNP) equation was derived for narrow and long pores with high aspect ratios, and the model quantitatively captured the experimental trends.[36] Another 1D PNP equation was developed using the perturbation theory that considers charge density renormalization and entropic effects, and it agreed well with experimental results under small-to-moderate ionic currents.[39] In recent works, a 1D PNP equation was derived to model nanopores connected with bulk reservoirs, and the maximum surface charge density it can treat is $-2.0\ e/\mathrm{nm}^2$ (e is the elementary charge), and a general trend was found that increasing the pore length increases the rectification ratios.[40] To model bulk reservoirs and access-resistance explicitly, 2D axisymmetric PNP equations have been used, and the results agree well with the experimental results. Previous research has also studied the effects of a nonuniformly charged pore wall and found that the position and thickness of the transition zone affect rectifications greatly.[41,42] In an experimental work,[37] the authors fabricated conical pores with various tip diameters (10−380 nm), studied their performance, and found general trends that decreasing ionic strength, decreasing tip diameter, and increasing surface charge density enhance rectifications. Rectification of $LiClO_4$, which is important to lithium ion battery technologies, in conical nanopores was studied using experiments and the PNP model.[43] It was found that the adsorption of lithium ions to pore walls and the dipole moment caused by the adsorbed molecules lead to the ion current rectification. Ion enrichment and ion depletion in nanopores are important to the conductance of the pore and the ion current rectification. In a recent experimental work,[15] by using time-dependent electrokinetic measurements, the extent of ion enrichment-depletion in conical nanopores over different time scales was quantitated from the area enclosed in the hysteresis current loops, and the dynamic ion concentration polarization was described with a simple capacitive charging model. An earlier experimental work[32] observed memcapacitive and memristive phenomena in single conical pores, and these phenomena were caused by finite ion mobility as ions redistribute in negatively charged pores in applied voltages.

Most prior research focused on the transport of dilute electrolytes in conical nanopores, while the transport of concentrated electrolytes was less studied. Room-temperature ionic liquids (RTILs) are a promising class of concentrated electrolytes. They are liquids at room temperature consisting entirely of ions. They have important properties such as excellent thermal stability, negligible vapor pressure, and a wide electrochemical window.[44,45] The interface between electrified surfaces and RTILs is crucial to electrochemical technologies; for example, EDLs at these interfaces can determine supercapacitors' capacitance.[46,47] For EDLs in RTILs, theoretical and experimental studies have shown interesting equilibrium properties such as overscreening and ions' alternative layering at the interfaces.[48−52] In terms of transport properties, most prior research studied the equilibrium properties of RTILs such as self-diffusion in nanopores,[53−57] while nonequilibrium properties of RTILs[58,59] were not widely studied. Recent work showed that EDLs can affect nonequilibrium transport of RTILs, and the associated phenomena are very different from those of dilute electrolytes.[60−62] For the transport of RTILs in conical nanopores, experiments were performed using negatively charged pores, and ion current rectifications were observed.[63] Large rectification ratios can be achieved by using a nonuniformly charged pore wall. These phenomena have been understood by using analysis similar to that for dilute electrolytes. Recently, a numerical work used a Landau−Ginzburg-type continuum model to study the current rectification for transport of RTILs through conical nanopores.[64] The continuum model was developed by Bazant, Storey, and Kornyshev (BSK) that takes the steric effect and strong ion−ion correlations into account.[52] It was found that the current rectification phenomena described by the BSK model agree qualitatively with the experimental results,[63] and the authors performed a quantitative analysis to explain the underlying physics for the observed phenomena.[64]

For the transport of RTILs in conical nanopores, there are still issues to be explored. First, the lengths of nanopores are from tens of nanometers to several micrometers in the numerical and experimental studies.[63,64] For nanopores with even smaller lengths, it is unknown whether the current rectification or ion enrichment-depletion will still happen. Although it is very difficult to fabricate a single conical nanopore with a length of a few nanometers, asymmetric and short nanopores exist in nanoporous electrodes of supercapacitors.[1] Confined electrolytes in these nanopores are connected with bulk-like electrolytes in larger pores, a scenario commonly found in nanoporous electrodes.[65] It is therefore important to study transport of RTILs in asymmetric and short pores under positive/negative biases, which is fundamental to charging/discharging nanoporous electrodes. The conical nanopore is used here as a prototype structure with broken symmetry. Second, recent molecular dynamics (MD) simulations showed nonlinear current−voltage (I−V) relationships and dewetting phenomenon in cylindrical nanopores with an access diameter of 2.17 nm.[61] It is unknown whether these phenomena will happen in conical nanopores as well. Third, although recent numerical work using the BSK model shows qualitative agreement with experimental results on current rectification for transport of RTILs through conical nanopores,[64] there are still approximations used in the continuum model. For example, the diffusion coefficients in the system were assumed constants. Prior MD simulations revealed that diffusion coefficients of RTILs in cylindrical pores with diameters <4 nm can be smaller than those in bulk;[56] the diffusion coefficients of RTILs were also showed to be concentration dependent.[61] It is then worthwhile to study the transport of RTILs in nanopores using MD simulations, because it makes no assumptions on parameters (e.g., diffusion coefficients) used in the continuum model. To address the above issues, MD simulations are used in this work to study the transport and structure of RTILs in a conical nanopore with a length of 10 nm connected with RTIL reservoirs. Ionic transports through electrically neutral, nonuniformly charged, and uniformly charged nanopores are studied and compared. Distributions of cation/anion number density, space charge density, and electrical potential in the systems are analyzed to explain the observations.

METHODS

MD simulations are used to study the ionic transport of the 1-butyl-3-methylimidazolium hexafluorophosphate ([BMIM]-[PF_6]) through conical nanopores driven by external electric fields. In the simulations, the equation of motion for N atoms is solved to move the atoms:

$$m_i \frac{\partial^2 \mathbf{r}_i}{\partial t^2} = \mathbf{F}_i,\ i = 1 \ldots N \tag{1}$$

https://dx.doi.org/10.1021/acs.jpcc.9b10201
J. Phys. Chem. C 2020, 124, 5817−5828

where t is time, and $\mathbf{r}_i$ and m_i are the coordinate and mass of atom i, respectively. The forces $\mathbf{F}_i$ on atom i are the sum of the negative derivative of total potential energy $U(\mathbf{r}_1, \mathbf{r}_2, ..., \mathbf{r}_N)$ and the force due to external electric field $\mathbf{E}_{ext}$:

$$\mathbf{F}_i = -\frac{\partial U}{\partial \mathbf{r}_i} + q_i \mathbf{E}_{ext} \tag{2}$$

where q_i is the charge on atom i. The pairwise potential energy is contributed by the Lennard-Jones (LJ) and the Coulomb interactions:

$$U_{ij}(r_{ij}) = 4\varepsilon_{ij}\left(\left(\frac{\sigma_{ij}}{r_{ij}}\right)^{12} - \left(\frac{\sigma_{ij}}{r_{ij}}\right)^{6}\right) + \frac{q_i q_j}{4\pi\varepsilon_0 r_{ij}} \tag{3}$$

where r_{ij} is the distance between atoms, ε_0 is the vacuum permittivity, and LJ parameters for the interaction between atom i and atom j are calculated as $\sigma_{ij} = (\sigma_i + \sigma_j)/2$ and $\varepsilon_{ij} = (\varepsilon_i \varepsilon_j)^{1/2}$ (Lorentz−Berthelot combination rule). Figure 1 shows a snapshot of the simulation system, and simulations are performed in the NVT ensemble using the Gromacs package.[68] Two vertical walls are boundaries of the reservoir to allow the RTIL to transport from one reservoir to the other through the pore only. The atoms of vertical walls are arranged in a square lattice with an atom spacing of 0.3 nm, and they are fixed during simulations. For the conical nanopore, two layers of the conical shell are modeled. The atoms in the inner layer are restrained to their fixed reference positions using position restraints provided by Gromacs, and they are the yellow atoms in Figure 1. The atoms in the outer layer are fixed, and they are the cyan atoms in Figure 1. In the case of a charged wall, only the atoms in the inner layer carry charges. The [BMIM][PF_6] is represented by a coarse-grained model,[69] and the model consists of a three-site cation and a single-site anion. For the cation sites (C1, C2, and C3) and the anion site (A), LJ parameter σ values are 0.438, 0.341, 0.504, and 0.506 nm, respectively, while LJ parameter ε values are 2.56, 0.36, 1.83, and 4.71 kJ/mol, respectively. Details of the model parameters are discussed in ref 69. The nanopore and vertical wall atoms are modeled as carbon atoms, and their LJ parameters are σ = 0.34 nm and ε = 0.36 kJ/mol.[70] The lengths of the nanopore and the RTIL reservoir along the nanopore axial direction (x direction) are both 10 nm. The diameters of the nanopore tip and base are 1.5 and 6.9 nm, respectively. Because the diameter of the wall atoms is 0.34 nm, the access diameter of the tip is 1.16 nm. The number of ions inside the system was adjusted so that the system is electrically neutral and the ion number density at the center of RTIL reservoir matches that of a bulk [BMIM][PF_6] at 400 K and 1 atm (2.68 nm^{-3}). Newton's equation of motion is integrated using the leapfrog algorithm. Temperatures of the RTILs and the atoms in the inner layer of the nanopore (yellow atoms in Figure 1) are maintained at 400 K using the velocity rescaling method with a time constant of 1 ps for ions and 0.25 ps for vibrating nanopore atoms. The smaller time constant for the nanopore atom is necessary to ensure that the heat generated during ionic transport is effectively dissipated. The Particle-Mesh-Ewald (PME) method is used to calculate electrostatic interactions with a real space cutoff of 1.6 nm and an FFT spacing of 0.12 nm. Nonelectrostatic interactions are computed using the cutoff method (cutoff radius: 1.6 nm). The neighbor list is updated each time step (2 fs). Bond lengths for RTIL ions are constrained using the LINCS algorithm[71] during the simulations. The PME method for electrostatic calculations requires that the system must be periodic in all three directions, except for the slab geometry, which is not the case in this study. Therefore, periodic boundary conditions (PBCs) are applied in all three directions. Applying PBCs in all three directions has been used to model ionic transport through nanopores by MD simulations.[72−74]

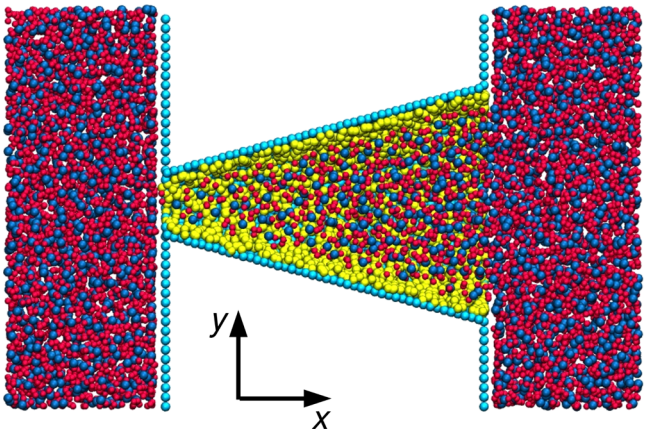

Figure 1. A snapshot of the MD simulation system. Red and blue spheres represent cations and anions, respectively; yellow and cyan spheres represent vibrating and fixed wall atoms, respectively. The lengths of the simulation box in the x, y, and z directions are 20.0, 12.6, and 12.6 nm, respectively. Periodic boundary condition is applied in all three directions. Visual Molecular Dynamics (VMD)[66,67] is used to generate the snapshot, where the system is clipped by the plane of symmetry in the z direction to better show the system's geometry and atoms inside the conical nanopore.

A voltage drop ϕ is imposed across the system to drive the ionic transport by applying a uniform electric field in the pore axial direction following $E_x = \phi/L_x$ (L_x is the length of the simulation system in the x direction). This method has been validated for ionic transport in various nanopores.[72,74,75] Although the external electric field is uniform, the electrical potential in the system conforms to the electrostatic law because of the reaction electric fields.[73,74] The total electrical potential is the sum of the potential due to the reaction electric fields and that associated with the uniform external field. At a given applied voltage, most of the potential drops near the pore tip; consequently, the total electric forces on ions near the pore tip are much larger than those elsewhere. ϕ is varied from −10 to 10 V in the simulations. In each simulation, a trial run of 5 ns is performed to reach a steady state, and then a production run of 40 ns is performed. Error bars are calculated from five independent cases. The method in ref 72 is used to calculate the ionic current. The displacement of the system's effective charge center is computed as

$$DC_c(t) = \left\langle \frac{1}{L_x}\sum_{i=1}^{N} q_i[x_i(t) - x_i(0)] \right\rangle \tag{4}$$

where N is the total number of RTIL atoms, $x_i(t \text{ or } 0)$ and q_i are the x position and charge of atom i, and $\langle\cdots\rangle$ is the ensemble average. The current is then calculated by a linear regression of $C_c(t)$. The position of each atom was recorded every 0.2 ps in simulations to compute the drift of the effective charge center $C_c(t)$.

https://dx.doi.org/10.1021/acs.jpcc.9b10201
J. Phys. Chem. C 2020, 124, 5817−5828

RESULTS AND DISCUSSION

Neutral Nanopore. Figure 2a shows the total ionic current along the x direction of the simulation system as a function of ϕ for neutral and charged conical nanopores. In the positive bias ($\phi > 0$), cations (anions) move from the nanopore tip (base) to the base (tip) and vice versa in the negative bias ($\phi < 0$). For the neutral nanopore, as $|\phi|$ increases, the ionic current increases nonlinearly with an increasing slope, indicating the system's ionic conductance increases as $|\phi|$ increases. This observation agrees with previous results for transport of RTILs in cylindrical nanopores.[61]

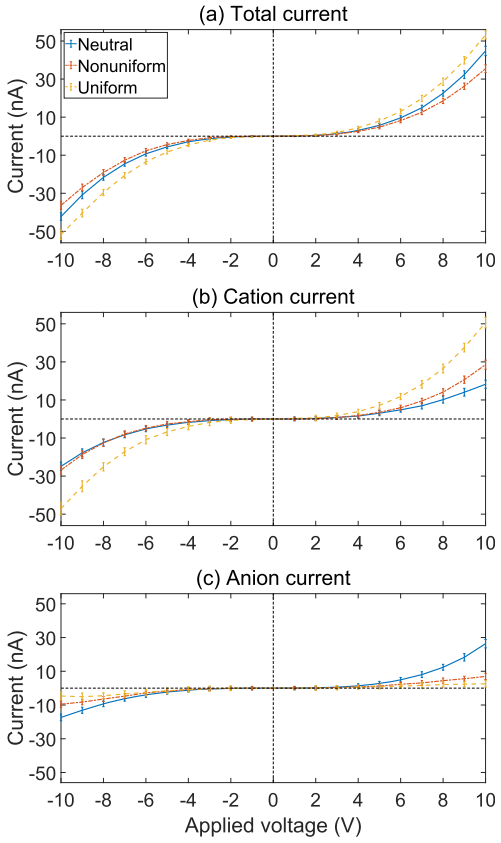

Figure 2. Ionic current as a function of applied voltage for the transport of RTILs in conical pores with various surface charge patterns. The total current, cation current, and anion current are shown in (a), (b), and (c), respectively. In the neutral case, the entire pore wall is electrically neutral. In the nonuniform case, the half of the pore wall near the tip is charged with a surface charge density of -0.2 C/m^2, while the other half near the base is electrically neutral. In the uniform case, the entire pore wall is charged with a surface charge density of -0.2 C/m^2.

To understand the nonlinearity of the $I-V$ relationship for transport of RTILs in conical nanopores, distributions of ion number density in the pores are analyzed. To calculate the ion number density, the nanopore is divided into five regions, and the length in the x direction of each region is 2 nm. The total numbers of cations and anions are averaged during simulations for each region, and they are then divided by each region's volume to obtain the average cation/anion number density. Figure 3 shows the average number density for cations and anions as a function of location in the x direction. The x coordinate of each data point is chosen to be the center of each region along the x direction. Under both positive and negative biases, the overall trend is that the cation/anion number density decreases in most regions as the magnitude of applied voltage increases. This is the ion depletion (dewetting in ref 61) phenomenon. When the concentrations of both cation and anion decrease given that the nanopore volume is constant, the volume of void (vacuum) increases in the nanopore. It physically means a process of dewetting and the nucleation of vapor bubbles (cavitation) inside the nanopore. This phenomenon has been reported for other liquids in prior experiments, continuum simulations, and MD simulations,[76,77] while their mechanisms are different from those in this study. The energy cost to dewet or create a vacuum in the highly viscous RTILs could be very high, and the dewetting phenomenon predicted here awaits experimental verification. The ion depletion and nonlinear $I-V$ relationship are consistent with those reported in ref 61, even though the types of pore wall atoms and the pore shapes are different. These phenomena can be understood as follows. Immediately after the voltage is applied, most of the voltage drop occurs near the nanopore tip in the pore. Consequently, the magnitude of the electric field near the tip is much larger than those in the bulk and near the base. Because the ionic

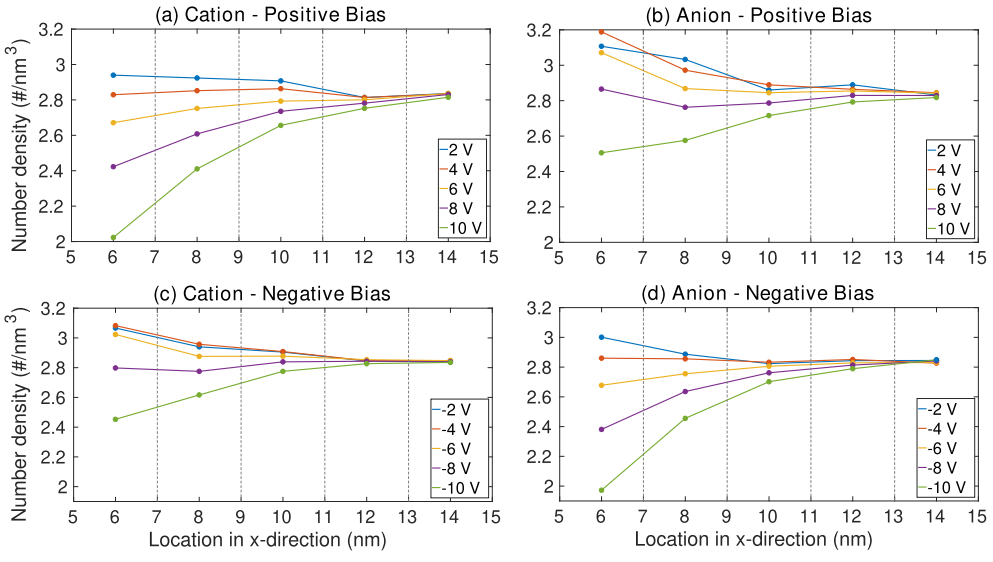

Figure 3. Distributions of cation and anion number density in the electrically neutral conical nanopore under different applied voltages.

https://dx.doi.org/10.1021/acs.jpcc.9b10201
J. Phys. Chem. C 2020, 124, 5817−5828

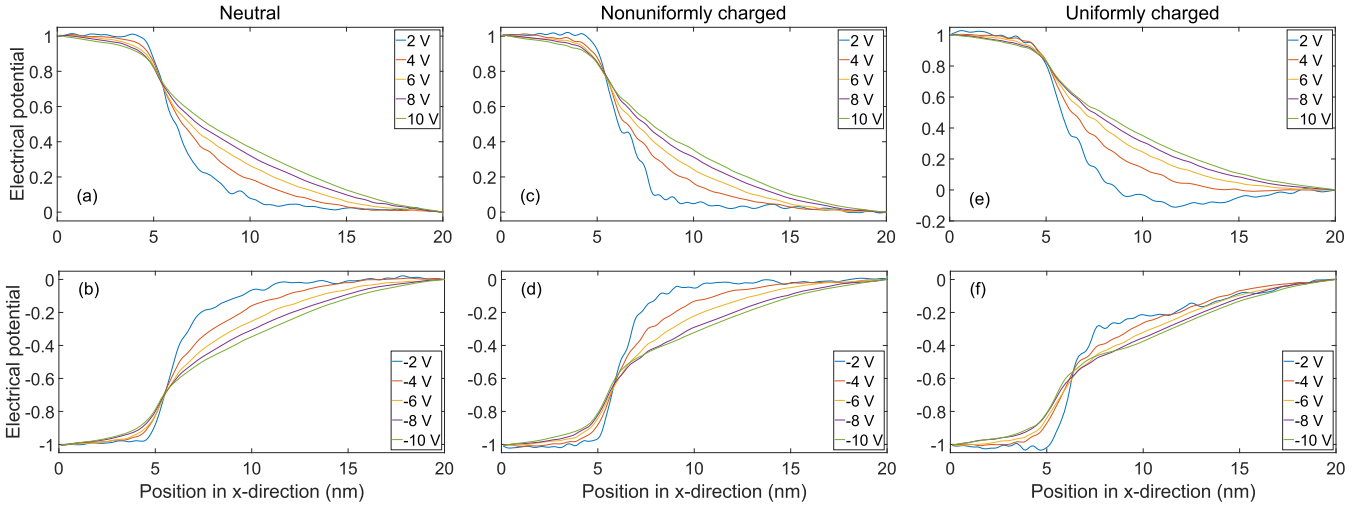

Figure 4. Electrical potential along the axial direction of the conical nanopore as a function of position in the x direction. Results are shown for different applied voltages in positive biases ((a), (c), and (e)) and negative biases ((b), (d), and (f)). Results for the neutral, nonuniformly charged, and uniformly charged pores are shown in the left, middle, and right panels, respectively. The electrical potential is scaled by the magnitude of applied voltage in each case.

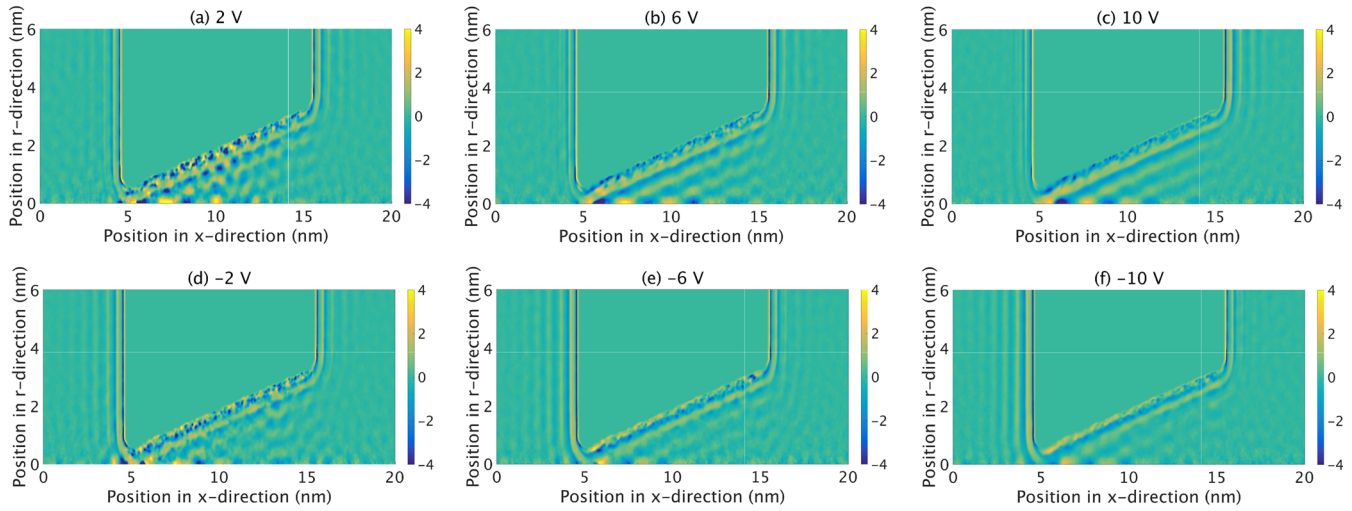

Figure 5. 2D axial-symmetric distributions of space charge density (e/nm^3) in the MD simulation system under different applied voltages. The nanopore is electrically neutral.

conductivity of RTILs increases as the magnitude of the electric field increases,[61] the ionic conductivity of RTILs near the tip can be larger than those of bulk RTILs and RTILs near the base. As a result, the ionic flux near the tip is larger than that elsewhere, leading to ion depletion near the tip. Ion depletion greatly enhances the ionic conductivity of RTILs and ionic flux near the tip, which is positive feedback. Accompanying the ion depletion is the building up of an ionic cloud near the entrance of the nanopore tip, which is evidenced by the increment in negative (positive) space charge density near the tip in the positive (negative) bias (see Figure 3). The ionic cloud lowers the voltage drop, electric field, and ionic flux near the tip, which is negative feedback. When the two feedbacks balance each other, the system reaches a steady state, and a stabilized ion depletion phenomenon establishes in the pore. As the applied voltage increases, the magnitude of the electric field increases and the degree of ion depletion increases. The above factors lead to the nonlinear increment in ionic conductivity of RTILs and ultimately the increasing ionic conductance of the system.

Changes in the ionic conductance of the nanopore can be observed directly by plotting the distribution of electrical potential along the nanopore axial direction (Figure 4). The electrical potential is calculated by using the VMD PMEPot plugin[72] and is scaled by the applied voltage in each case. One notable feature of Figure 4 is that, under both positive and negative biases, the gradient of electrical potential near the nanopore tip decreases as the magnitude of applied voltage increases, indicating the increase in ionic conductance near the tip. It is also observed that for the small voltage (2 V), the electric potential increases around x = 4 nm; for other voltages, it decreases. For the small voltage (2 V), the magnitude of the electric field around x = 4 nm due to the applied voltage is smaller than that due to space charges. Thus, the nonzero space charge density around x = 4 nm (see Figure 5a) dominates in that region and causes the electric potential to increase. For other voltages, the magnitude of the electric field due to the applied voltage becomes considerably larger than that due to space charges. As a result, the applied voltage dominates in that

https://dx.doi.org/10.1021/acs.jpcc.9b10201
J. Phys. Chem. C 2020, 124, 5817−5828

region, causing the electric potential to decrease around x = 4 nm.

One feature of the ion depletion is that it is inhomogeneous: the degree of ion depletion decreases as the location moves from the tip to the base. Figure 3 shows that the degree of ion depletion is highest near the tip; near the base, cation/anion number density remains nearly unchanged as the applied voltage increases. The inhomogeneous ion depletion can be understood as follows. As the location moves from the tip to the base, the nanopore radius becomes larger and RTILs are more bulk-like. Figure 4 indicates that the magnitude of the electric field decreases from the tip to the base. Near the base, the electric field is almost the same as that in the reservoir, and variations in the magnitude of electric field and ionic conductivity are relatively small. Thus, immediately after the voltage is applied, the ionic flux in the x direction is more uniform near the base, and it is more difficult to trigger the ion depletion process. Moreover, even if the ion depletion is triggered, the sharp increase of ionic conductivity as the ion concentration reduces is difficult to achieve because RTILs are more bulk-like near the base. It was reported that when the density of bulk RTILs is reduced by 20%, their ionic conductivity only increases slightly.[61] Although the higher ionic conductivity triggers ion depletion, the electric field in the nanopore decreases quickly due to the screening of the electric field by ionic clouds. Because ionic conductivity only increases slightly as the ion concentration decreases, the decrease of electric field in the nanopore halts the growth of ionic clouds and ion depletion near the base. As a result, ion depletion becomes weaker as the location moves from the tip to the base, and Figure 3 shows that it is extremely weak near the base. Note that the 2 and 4 V cases show more cations near the tip than near the base. Similar behaviors are observed for anions from 2 to 8 V, cations from −2 to −6 V, and anions at −2 and −4 V. These are because ions near the tip are basically in EDLs (see Figure 5), while ions near the base are nearly in bulk. In the aforementioned cases, the effect of EDL formation near the tip is more significant than that of ion depletion, so ion concentration is higher than that near the base. One consequence of the inhomogeneous ion depletion is that the nonequilibrium diffusion coefficients of RTILs are inhomogeneous in the pore: they are largest near the tip and become close to their bulk values near the base, because diffusion coefficients increase as ion concentrations decrease in RTILs.[62,64] This is in contrast to those in the equilibrium condition, where diffusion coefficients of RTILs are smaller near the tip because they decrease as the nanopore becomes narrower.[55]

In Figure 3, it is also observed that, when the applied voltage increases from 2 to 10 V, the degree of ion depletion for the cation is higher than that for the anion near the tip: the cation number density decreases from 2.94 to 2.02 nm^{-3} with a reduction of 31.3%, while the anion number density decreases from 3.11 to 2.50 nm^{-3} with a reduction of 19.6%. In negative biases, the trend is the opposite: the cation number density decreases from 3.07 to 2.45 nm^{-3} with a reduction of 20.2%, while the anion number density decreases from 3.00 to 1.97 nm^{-3} with a reduction of 34.3%. The above observations can be rationalized by examining how ionic clouds form near the tip under different biases. Under positive biases, cations (anions) move from the tip (base) to the base (tip); thus anions accumulate near the tip while cations are depleted from this region, forming a negatively charged ionic cloud near the tip. In negative biases, cations (anions) move from the base (tip) to the tip (base); thus cations accumulate near the tip while anions are depleted from this region, forming a positively charged ionic cloud. Consequently, when the applied voltage increases, the cation (anion) number density reduces more than that of the anion (cation) in positive (negative) biases. The competition between ionic cloud formation and ion depletion can lead to nonmonotonic changes in ion concentration near the tip as the applied voltage increases. Figure 3b shows that, when the applied voltage increases from 2 to 4 V, the anion number density very close to the tip increases. This is because the effect of anion cloud formation near the tip is more important than that of ion depletion. In negative biases, similar behavior is observed for cations when the applied voltage changes from −2 to −4 V, because the effect of cation cloud formation is more important.

The 2D axial-symmetric distribution of space charge density in the simulation system is also analyzed. Figure 5 shows the results. Even though the pore is electrically neutral, EDLs form near the pore wall. This is because the external electric field has a component perpendicular to the pore wall. In positive (negative) biases, anions (cations) dominate in the first layer near the pore wall, because the external electric field drives anions (cations) more toward the wall. As the applied voltage varies, the EDL structure changes. When $|\phi| = 2$ V (see Figure 5a and d), a mixture of cations and anions is observed in each layer of EDLs, because the magnitude of external electric field is not very large and is comparable to that of the field from ion−ion correlations in RTILs. Nonetheless, cations and anions still dominate in the first and second layers, respectively. Because the spacing between adjacent wall atoms is large and the nanopore surface is rough, spot-like accumulations of cations and anions are observed in EDLs. When the $|\phi|$ values are 6 and 10 V (see Figure 5b, c, e, and f), the external electric field is stronger to separate cations and anions; thus the EDL structures become more distinguishable, and the interface between neighboring layers becomes smoother. Another feature of EDLs in the neutral pore is that the magnitude of space charge density near the tip is generally larger than that near the base, because most of the voltage drop occurs near the tip and the electric field is stronger.

For the current rectification phenomenon, the rectification ratio at $\pm\phi$ is calculated by $|I_{+\phi}/I_{-\phi}|$. The ratio is 1.06 at ±10 V, indicating extremely weak rectification. Prior experimental and numerical studies suggested that increasing the nanopore length increases the rectification ratios.[38,40] The very weak rectification observed above is likely due to the fact that the length of the conical nanopore in this study is 10 nm and is orders of magnitude shorter than 12 μm-long nanopores in experiments where the rectification ratio for the neutral pore is 1.48 at ±5 V.[63]

Charged Nanopores. *Nonuniformly Charged Nanopore.* Ionic transport of RTILs through charged conical nanopores is also studied. In this case, the pore wall is nonuniformly charged: the half of the pore wall near the tip is charged with a surface charge density of −0.2 C/m^2; the other half near the base is electrically neutral. The purpose for using this surface charge pattern is to test whether the rectification ratio can be enhanced or not for the system in this study, because earlier experimental and numerical studies showed that this nonuniform surface charge pattern can be used to enhance the rectification ratio.[63,64] Another reason to use the nonuniform surface charge distribution on the pore wall is because it better matches experimental conditions where surface chemistry (deprotona-

https://dx.doi.org/10.1021/acs.jpcc.9b10201
J. Phys. Chem. C 2020, 124, 5817−5828

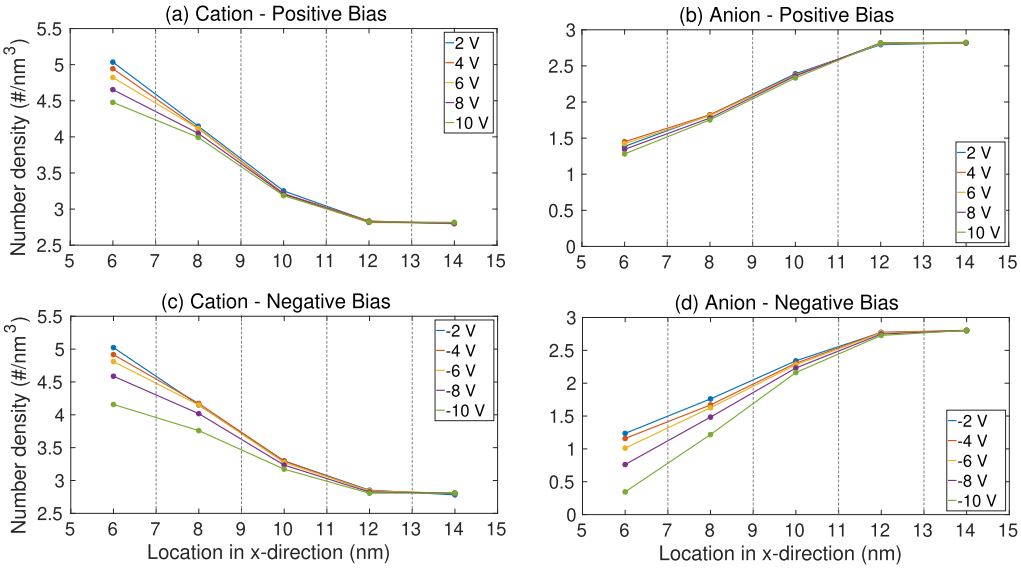

Figure 6. Distributions of cation and anion number density in the nonuniformly charged conical nanopore under different applied voltages. The half of the pore wall near the tip is electrically charged, and the other half near the base is electrically neutral.

tion of functional groups) occurs under external electric fields.[78] The relatively high surface charge density of -0.2 C/m^2 is chosen to induce higher ion concentrations near the tip and to study its effect on ionic transport through the pore. Note that the nanopore in this study is made of carbon, and the magnitude of surface charge density considered here is smaller than that reported in ref 79 (-0.23 C/m^2) for studying EDLs in RTILs near carbon electrodes. The red dashed lines in Figure 2 are the $I-V$ relationships for the nonuniformly charged conical nanopore. It shows that the rectification is still very weak, indicating that the effect of the nanopore length may play a dominant role here. It is desirable to study the effect of the length on the rectification using MD simulations. To perform systematic investigations and obtain a thorough understanding of the length effect, the nanopore length can be varied from a few nanometers to several micrometers. The longest nanopore should be several micrometers long, such that significant current rectification can be achieved.[63] However, in an MD simulation system containing a 1 μm-long conical nanopore filled with coarse-grained RTIL molecules, the total number of atoms is estimated to be on the order of billions. The huge computational cost of MD simulations for such systems prevents a systematic study on the length effect.

Figure 2a shows that, for the nonuniformly charged conical nanopore, the magnitude of ionic current increases nonlinearly with an increasing slope as the magnitude of applied voltage increases. This is consistent with that for the neutral pore in this study and those in ref 61. Cation and anion currents are calculated separately, and the results are shown in Figure 2b and c. It is observed that the cation current is increased while the anion current is decreased notably in the negatively charged pore as compared to those in the neutral pore at a certain applied voltage. This indicates that the negatively charged pore is selective: it promotes transport of cations while it hinders transport of anions through the pore. The nonlinear $I-V$ relationship can be understood by using a similar analysis for the neutral conical pore: in both positive and negative biases, cation/anion number density decreases near the tip as the applied voltage increases (see Figure 6); the ion depletion enhances the ionic conductivity of RTILs near the tip, and ultimately the system's ionic conductance is increased as the applied voltage becomes stronger. It is also observed that the cation number density in the negatively charged nanopore is increased as compared to that in the neutral nanopore, which reflects the defined surface charges because the number density is calculated when the simulation system reaches a steady state under a fixed applied voltage. This is different from results in time-dependent studies on hysteresis charges.[15] It would be desirable to apply time-dependent voltages and study current–voltage loops and possibly the hysteresis phenomena for systems considered in this work. Given that the focus of this work is on transport phenomena at steady states, time-dependent investigations following those in ref 15 would be performed in future studies.

In Figure 2a, it is observed that the magnitude of total current through the nonuniformly charged pore is smaller than that through the neutral pore at the same applied voltage. To understand this phenomenon, ion concentrations in the two cases are compared. The ion depletion occurs in both neutral and charged pores; however, the length in the x-direction of the ion depletion region and the degree of ion depletion are different. In the neutral pore, Figure 3 shows that obvious ion depletion occurs when $x < 14$; while in the nonuniformly charged pore, Figure 6 shows that obvious ion depletion occurs when $x < 12$. Thus, the ion depletion region's length in the neutral pore is longer. For the degree of ion depletion, when the applied voltage increases from 2 to 10 V in the charged pore, the total ion number density near the tip decreases from 6.41 to 5.76 nm^{-3} with a reduction of 10.1%; in negative biases, it decreases from 6.26 to 4.51 nm^{-3} with a reduction of 27.9%. In the neutral pore, when the applied voltage increases from 2 to 10 V, the total ion number density near the tip decreases from 6.05 to 4.52 nm^{-3} with a reduction of 25.3%; in negative biases, it decreases from 6.07 to 4.42 nm^{-3} with a reduction of 27.2%. These results show that the degree of ion depletion in the nonuniformly charged pore is lower than that in the neutral pore. Because of the relatively high surface charge density and strong ion–ion correlations in RTILs, ions in the charged pore are more difficult to be depleted, and the total ion concentration in the charged pore is higher than that in the neutral pore. The above factors

https://dx.doi.org/10.1021/acs.jpcc.9b10201
J. Phys. Chem. C 2020, 124, 5817–5828

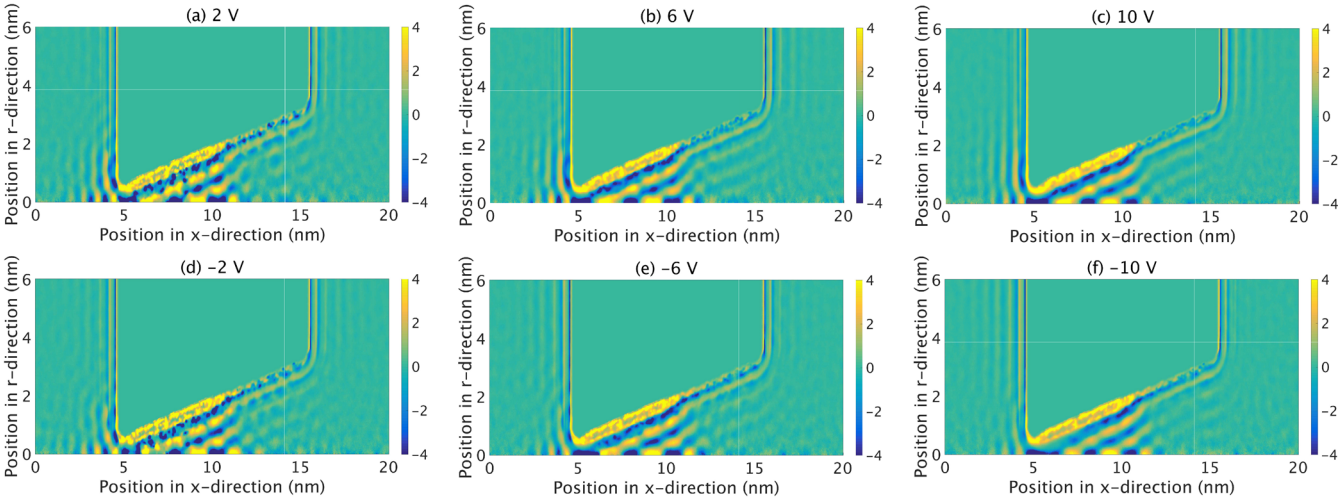

Figure 7. 2D axial-symmetric distributions of space charge density (e/nm^3) in the MD simulation system under different applied voltages. The half of the pore wall is negatively charged near the tip with a surface charge density of −0.2 C/m^2, while the other half near the base is electrically neutral.

lead to the smaller ionic conductivity in the nonuniformly charged pore and consequently the smaller current.

The above observation is opposite to that in ref 61 where the magnitude of ionic current through the charged cylindrical nanopore is greatly enhanced as compared to that through the neutral cylindrical nanopore. For the charged cylindrical pore, significant ion depletion occurs nearly in the entire pore;[61] while for the charged conical pore, significant ion depletion occurs only near the tip. Furthermore, in the charged cylindrical pore, directions of the external electric field and associated ionic transport are parallel to the pore wall and the interface between neighboring layers in EDLs. The alternative layering of EDLs can greatly enhance ionic transport through the pore.[60,61] Thus, ionic conductivity of the charge cylindrical pore is much larger than that of the neutral cylindrical pore, which leads to the enhanced current through the charged cylindrical pore.

Figure 4c and d shows the distribution of electrical potential along the axial direction of the pore in the system. It is observed that most of the potential drop occurs near the tip, due to the fact that the tip diameter is the smallest in the pore and is smaller than the lateral dimension of the RTIL reservoir. In both positive and negative biases, the amount of voltage drop across the pore decreases as the applied voltage increases, indicating that the ionic conductance of the pore increases. These observations are consistent with those in the neutral pore system. Oscillations of electrical potential are observed, and they are caused by the EDLs formed in the pore. Because of the higher peak values of the space charge density (compare Figures 5 and 7) induced by surface charges on the pore wall, the oscillations are more pronounced in the charged pore system.

The distributions of space charge density in the nonuniformly charged conical nanopore system under different applied voltages are shown in Figure 7. Because of the negative surface charges near the tip, distinct EDL formation is observed in this region. Although the half of the pore wall near the base is electrically neutral, EDL formation is also observed because of the effect from the external electric field. Near the tip, the peak value of the space charge density in EDLs is larger than those near the base. These are because electric forces acting on ions that originate from surface charges are larger than those from the external electric field. Near the base and in positive biases, although cations move away from the wall under the external electric field, there are still cations in the first layer of EDLs near the wall because of the attraction from negative surface charges near the tip; as the external electric field becomes stronger, the amount of cations in the first layer near the base decreases. In negative biases, cations are always in the first layer of EDLs near the base because of the cooperative effects from negative surface charges and the external electric field. In Figure 7, "void" space between ion layers is observed. As the space charge density is computed by subtracting negative space charge density from positive density, although this charge density can be zero at certain positions in this "void" space, it does not necessarily mean that the ion concentration is zero. There are still ions in the "void" space between ion layers shown in Figure 7, while the ion concentration there is smaller than that in the density peaks of the ion layers.[80] The electrical potential energy has local maxima/minima at positions of density peaks, and it changes from maxima (minima) to minima (maxima) in the "void" space between ion layers; the electrical forces thus reach local maxima in those "void" spaces.[80]

Uniformly Charged Nanopore. Transport of RTILs through the uniformly charged nanopore is also studied, and the surface charge density is the same as that for the nonuniformly charged nanopore. Figure 2a shows the nonlinear $I-V$ relationship and weak rectifications that are consistent with results for neutral and nonuniformly charged nanopores. However, the magnitude of ionic current at a certain applied voltage is larger than that for the neutral pore; this is opposite to the result for the nonuniformly charged pore. There are mainly two factors affecting the ionic transport of RTILs through the nanopore. On the one hand, when the pore is uniformly charged, EDLs form in the entire pore (see Figure 9) that enhance ionic transport parallel to the pore wall and facilitate the ion depletion; on the other hand, the larger total ion concentration and lower degree of ion depletion due to surface charges reduce the ionic conductivity of the pore, which hinders ionic transport through the pore. In the uniformly charged pore, the enhanced transport due to EDL formation plays a dominant role so that the current is larger than those in the neutral and nonuniformly charged pores at a certain applied voltage. Note that the enhancement of ionic current through the uniformly charged conical nanopore is less significant than that through the uniformly charged cylindrical nanopore reported in ref 61. In the cylindrical nanopore, the external electric field is

https://dx.doi.org/10.1021/acs.jpcc.9b10201
J. Phys. Chem. C 2020, 124, 5817−5828

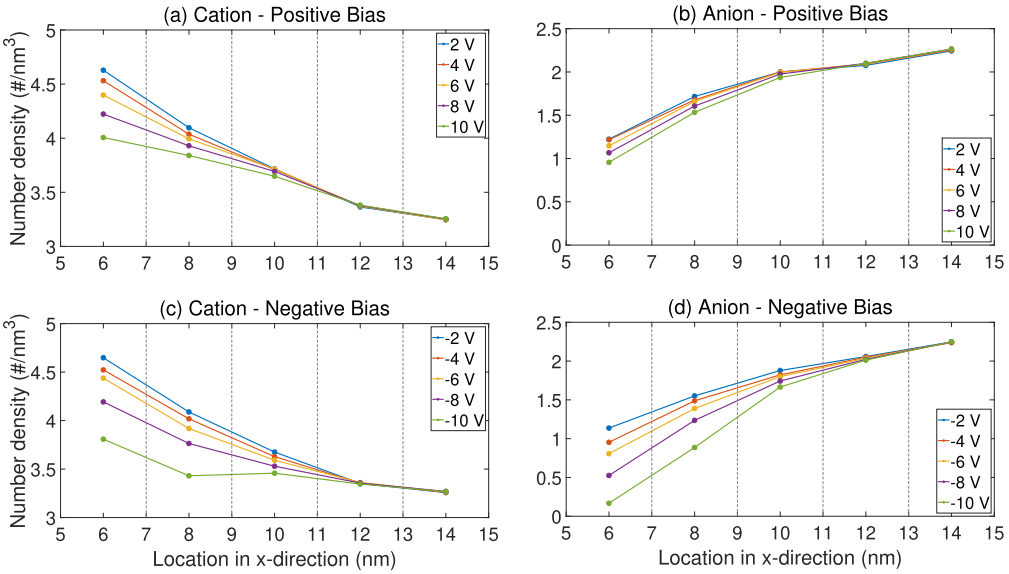

Figure 8. Distributions of cation and anion number density in the uniformly charged conical nanopore under different applied voltages.

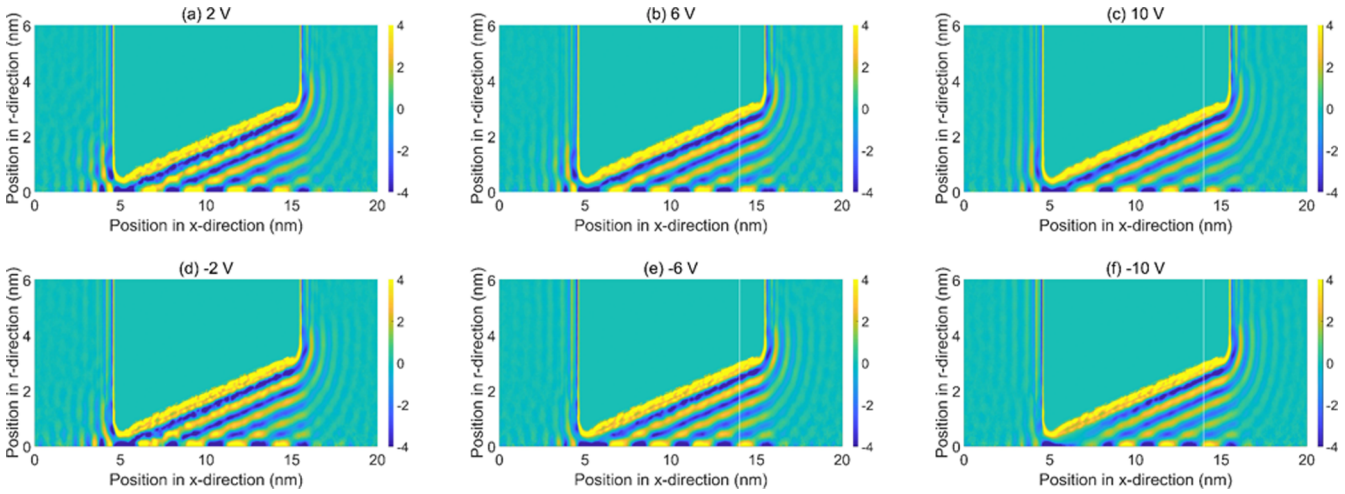

Figure 9. 2D axial-symmetric distributions of space charge density (e/nm^3) in the MD simulation system under different applied voltages. The pore wall is uniformly charged.

parallel to the pore wall and the interface between neighboring layers in EDLs, which greatly facilitates ionic transport of RTILs and induces significant ion depletion in the entire pore; while in the conical nanopore, although EDLs form in the entire pore and ionic transport parallel to the pore wall is enhanced, significant ion depletion occurs only near the tip, and thus the increment of ionic conductivity of the conical pore is less than that of the cylindrical pore. From Figure 2b and c, it is also observed that the cation current is increased and the anion current is decreased as compared to those for both neutral and nonuniformly charged pores. The selective transport of cations through the pore is enhanced because of the uniform negative surface charges on the pore wall.

Distributions of cation and anion number density in the uniformly charged nanopore under different applied voltages are shown in Figure 8. The ion number density decreases in most regions of the pore as the applied voltage increases, and the ion depletion is most significant near the tip. These results are similar to those in the nonuniformly charged pore. At a certain applied voltage, the ion number density in the uniformly charged pore is slightly smaller than that in the nonuniformly charged pore. Because the formation of EDLs in the entire pore greatly enhances ionic transport of RTILs through the pore, immediately after the voltage is applied, the ionic flux through the uniformly charged pore is larger, which facilitates the ion depletion in the pore. As a result, when the systems reach steady states, the degree of ion depletion in the uniformly charged pore is higher than that in the nonuniformly charged pore.

Distributions of electrical potential along the axial direction of the uniformly charged pore are shown in Figure 4e and f. As the applied voltage increases, the gradient of electrical potential decreases near the tip because the ionic conductivity increases in this region. This result is consistent with those for neutral and nonuniformly charged pores. When the applied voltage is relatively small (for example, at ±2 V), the electrical potentials near the base are notably smaller than those in neutral and nonuniformly charged pores. This is because surface charges on the entire pore wall have a greater influence on electrical potentials in the pore than does the external electric field at smaller applied voltages. However, as the applied voltage increases, the external electric field becomes stronger, so

https://dx.doi.org/10.1021/acs.jpcc.9b10201
J. Phys. Chem. C 2020, 124, 5817−5828

differences in the electrical potential between different surface charge patterns become smaller.

Figure 9 shows the distributions of space charge density in the simulation system under different applied voltages for the uniformly charged pore. Because the pore wall is uniformly charged, EDLs form in the entire pore. The changes in the EDL structure inside the uniformly charged nanopore are marginal between most of the applied voltages considered in this study. However, when the applied voltage is −10 V, the magnitude of negative space charge density in the second layer of EDLs decreases notably near the tip. Because most of the ions in the second layer are anions, the motion/force on the anion is analyzed as follows. On the one hand, anions in this case move from the tip to the base under the influence of the external electric field; on the other hand, anions are attracted by cations in the first layer of EDLs near the pore wall. When the applied voltage is −10 V, the external electric field near the tip is so strong that forces on anions due to the external electric field are larger than attractive forces on anions due to the first layer of EDLs. As a result, anion concentration decreases, and the second layer of EDLs is driven apart from the first layer near the tip.

CONCLUSIONS

Nonequilibrium transport and structure of RTILs in conical nanopores under external electric fields were studied using MD simulations. Electrically neutral, nonuniformly charged, and uniformly charged nanopores were considered. The $I-V$ relationship was calculated as the macroscopic transport property. Under positive and negative biases, as the magnitude of applied voltage increases, the magnitude of current through the system increases nonlinearly with an increasing slope, and the ion concentration decreases in the pore. Because the ionic conductivity of RTILs increases as the magnitude of electric field increases and as the ion concentration decreases due to the solvent-free nature of RTILs,[61] the system's conductance increases as the applied voltage increases, and the $I-V$ curves are nonlinear. The degree of ion depletion in the pore is highest near the tip and decreases as the location moves from the tip to the base. The inhomogeneous ion depletion results from the symmetry-breaking geometry of the conical pore and the nonuniform electric field and RTILs' conductivity in the pore. EDLs were observed near pore walls, and the results suggest that the ion density in EDLs is tunable by varying the applied voltage.

The current through the nonuniformly charged pore was found to be weaker than that through the neutral pore at the same applied voltage. In this case, the total ion concentration is higher and the degree of ion depletion is lower than those in the neutral pore due to the surface charge effect and strong ion−ion correlations in RTILs. These cause the ionic conductivity of RTILs in the charged pore to decrease. On the other hand, the enhanced ionic transport parallel to the charged surface due to EDL formations plays a minor role here, because significant EDL formations only occur near the tip. For the uniformly charged pore, the current is stronger than that through the neutral pore at the same applied voltage. As EDLs form in the entire pore, the enhanced ionic transport parallel to the charged surface becomes dominant. The cation and anion currents were calculated separately. In the nonuniformly charged pore, the cation (anion) current is larger (smaller) than that in the neutral pore; in the uniformly charged pore, the cation (anion) current is further increased (decreased) as compared to that in the nonuniformly charged pore. These results show that negatively charged pores are cation-selective, and increasing the amount of surface charges enhances selective transport.

It was also found that ionic current rectifications are extremely weak in all cases, likely due to the fact that the nanopore length is orders of magnitude smaller than those in experiments, because prior studies showed that increasing the nanopore length can enhance the rectification ratios. Nonetheless, the relatively short conical nanopores studied in this work could be found in nanoporous electrodes, and studying the transport of RTILs through these nanopores can help understand transport phenomena that underpin electrical energy storage applications. Although the pore does not rectify in the presence of RTILs, it implies that total currents are similar under charging and discharging conditions in nanoporous electrodes. On the other hand, MD simulations of such a system can also provide physical insights at the molecular level for further improving continuum models that describe transport of strongly correlated electrolytes. For example, concentration-dependent diffusion coefficients and electric field-dependent mobility can be incorporated into the BSK model to better describe the nonlinear transport phenomena of RTILs in nanopores with geometries similar to that in this study. It is also desirable to perform comparisons between MD simulations and the BSK model on the transport of RTILs through nanopores. The BSK model is parametrized using properties of the model RTILs in which the cation and anion are spheres with the same size.[51] The $[BMIM^+]$ and $[PF_6^-]$ used in this study have different sizes and molecular details, which prevents a good comparison between MD simulations and the BSK model. Future work may use the model RTILs in MD simulations to compare to the BSK model.

Mechanisms revealed in this work for the inhomogeneous ion depletion and differences in the current between neutral and charged pores provide insights on the transport of RTILs in conical nanopores. These physical insights demonstrate the importance of solvent-free nature and strong ion−ion correlations in RTILs on their nonequilibrium transport and structures in nanopores, and the results imply that the charging dynamics of RTILs in nanoporous electrodes in supercapacitor and energy applications could be greatly enhanced under larger applied voltages. A fundamental understanding of these phenomena not only lays the ground for fully exploiting the potential of RTILs in applications such as energy storage and nanopore sensing techniques, but also helps to illuminate other complex phenomena in the nonequilibrium transport of concentrated electrolytes in nanopores.

AUTHOR INFORMATION

Corresponding Author

Xikai Jiang − *State Key Laboratory of Nonlinear Mechanics, Institute of Mechanics, Chinese Academy of Sciences, Beijing 100190, China;* orcid.org/0000-0001-5601-8339; Email: xikaij@imech.ac.cn

Complete contact information is available at: https://pubs.acs.org/10.1021/acs.jpcc.9b10201

Notes

The author declares no competing financial interest.

ACKNOWLEDGMENTS

I am thankful for support from the Institute of Mechanics, Chinese Academy of Sciences (CAS), the CAS Strategic Priority Research Program (XDB22040403), and the CAS Key Research

Program of Frontier Sciences (QYZDB-SSW-JSC036). Computing resources were provided by the National Supercomputer Center in Tianjin.

REFERENCES

(1) Merlet, C.; Rotenberg, B.; Madden, P. A.; Taberna, P.-L.; Simon, P.; Gogotsi, Y.; Salanne, M. On the Molecular Origin of Supercapacitance in Nanoporous Carbon Electrodes. *Nat. Mater.* **2012**, *11*, 306.

(2) Choi, N.-S.; Chen, Z.; Freunberger, S. A.; Ji, X.; Sun, Y.-K.; Amine, K.; Yushin, G.; Nazar, L. F.; Cho, J.; Bruce, P. G. Challenges Facing Lithium Batteries and Electrical Double-Layer Capacitors. *Angew. Chem., Int. Ed.* **2012**, *51*, 9994−10024.

(3) Beidaghi, M.; Gogotsi, Y. Capacitive Energy Storage in Micro-Scale Devices: Recent Advances in Design and Fabrication of Micro-Supercapacitors. *Energy Environ. Sci.* **2014**, *7*, 867−884.

(4) Li, W.; Liu, J.; Zhao, D. Mesoporous Materials for Energy Conversion and Storage Devices. *Nat. Rev. Mater.* **2016**, *1*, 16023.

(5) Gao, J.; Guo, W.; Feng, D.; Wang, H.; Zhao, D.; Jiang, L. High-Performance Ionic Diode Membrane for Salinity Gradient Power Generation. *J. Am. Chem. Soc.* **2014**, *136*, 12265−12272.

(6) Zhang, Z.; Kong, X.-Y.; Xiao, K.; Liu, Q.; Xie, G.; Li, P.; Ma, J.; Tian, Y.; Wen, L.; Jiang, L. Engineered Asymmetric Heterogeneous Membrane: A Concentration-Gradient-Driven Energy Harvesting Device. *J. Am. Chem. Soc.* **2015**, *137*, 14765−14772.

(7) Zhang, Z.; Sui, X.; Li, P.; Xie, G.; Kong, X.-Y.; Xiao, K.; Gao, L.; Wen, L.; Jiang, L. Ultrathin and Ion-Selective Janus Membranes for High-Performance Osmotic Energy Conversion. *J. Am. Chem. Soc.* **2017**, *139*, 8905−8914.

(8) Lee, R. C.; Hannig, J. In *Membrane Biology and Biophysics*; Souba, W. W., Wilmore, D. W., Eds.; Academic Press: San Diego, CA, 2001; Chapter 25, pp 297−305.

(9) Schoch, R. B.; Han, J.; Renaud, P. Transport Phenomena in Nanofluidics. *Rev. Mod. Phys.* **2008**, *80*, 839−883.

(10) Kim, S. J.; Wang, Y.-C.; Lee, J. H.; Jang, H.; Han, J. Concentration Polarization and Nonlinear Electrokinetic Flow near a Nanofluidic Channel. *Phys. Rev. Lett.* **2007**, *99*, 044501.

(11) Dydek, E. V.; Bazant, M. Z. Nonlinear Dynamics of Ion Concentration Polarization in Porous Media: The Leaky Membrane Model. *AIChE J.* **2013**, *59*, 3539−3555.

(12) abu Rjal, R.; Chinaryan, V.; Bazant, M. Z.; Rubinstein, I.; Zaltzman, B. Effect of Concentration Polarization on Permselectivity. *Phys. Rev. E* **2014**, *89*, 012302.

(13) Cao, L.; Wen, Q.; Feng, Y.; Ji, D.; Li, H.; Li, N.; Jiang, L.; Guo, W. On the Origin of Ion Selectivity in Ultrathin Nanopores: Insights for Membrane-Scale Osmotic Energy Conversion. *Adv. Funct. Mater.* **2018**, *28*, 1804189.

(14) Pu, Q.; Yun, J.; Temkin, H.; Liu, S. Ion-Enrichment and Ion-Depletion Effect of Nanochannel Structures. *Nano Lett.* **2004**, *4*, 1099−1103.

(15) Wang, D.; Brown, W.; Li, Y.; Kvetny, M.; Liu, J.; Wang, G. Hysteresis Charges in the Dynamic Enrichment and Depletion of Ions in Single Conical Nanopores. *ChemElectroChem* **2018**, *5*, 3089−3095.

(16) Wang, G.; Brown, W.; Kvetny, M. Structure and Dynamics of Nanoscale Electrical Double Layer. *Curr. Opin. Electrochem.* **2019**, *13*, 112−118.

(17) Siwy, Z. Ion-Current Rectification in Nanopores and Nanotubes with Broken Symmetry. *Adv. Funct. Mater.* **2006**, *16*, 735−746.

(18) Karnik, R.; Duan, C.; Castelino, K.; Daiguji, H.; Majumdar, A. Rectification of Ionic Current in a Nanofluidic Diode. *Nano Lett.* **2007**, *7*, 547−551.

(19) White, H. S.; Bund, A. Ion Current Rectification at Nanopores in Glass Membranes. *Langmuir* **2008**, *24*, 2212−2218.

(20) Guo, W.; Xia, H.; Xia, F.; Hou, X.; Cao, L.; Wang, L.; Xue, J.; Zhang, G.; Song, Y.; Zhu, D.; et al. Current Rectification in Temperature-Responsive Single Nanopores. *ChemPhysChem* **2010**, *11*, 859−864.

(21) Liu, J.; Kvetny, M.; Feng, J.; Wang, D.; Wu, B.; Brown, W.; Wang, G. Surface Charge Density Determination of Single Conical Nanopores Based on Normalized Ion Current Rectification. *Langmuir* **2012**, *28*, 1588−1595.

(22) Lan, W.-J.; Edwards, M. A.; Luo, L.; Perera, R. T.; Wu, X.; Martin, C. R.; White, H. S. Voltage-Rectified Current and Fluid Flow in Conical Nanopores. *Acc. Chem. Res.* **2016**, *49*, 2605−2613.

(23) Maass, P.; Bunde, A.; Ingram, M. D. Ion Transport Anomalies in Glasses. *Phys. Rev. Lett.* **1992**, *68*, 3064−3067.

(24) Heil, S. R.; Holz, M. Electrical Transport in a Disordered Medium: NMR Measurement of Diffusivity and Electrical Mobility of Ionic Charge Carriers. *J. Magn. Reson.* **1998**, *135*, 17−22.

(25) Bisquert, J.; Garcia-Belmonte, G.; Fabregat-Santiago, F.; Compte, A. Anomalous Transport Effects in the Impedance of Porous Film Electrodes. *Electrochem. Commun.* **1999**, *1*, 429−435.

(26) Padma Kumar, P.; Yashonath, S. Ion Mobility and Levitation Effect: Anomalous Diffusion in Nasicon-Type Structure. *J. Phys. Chem. B* **2002**, *106*, 3443−3448.

(27) OHern, S. C.; Boutilier, M. S. H.; Idrobo, J.-C.; Song, Y.; Kong, J.; Laoui, T.; Atieh, M.; Karnik, R. Selective Ionic Transport through Tunable Subnanometer Pores in Single-Layer Graphene Membranes. *Nano Lett.* **2014**, *14*, 1234−1241.

(28) Rollings, R. C.; Kuan, A. T.; Golovchenko, J. A. Ion Selectivity of Graphene Nanopores. *Nat. Commun.* **2016**, *7*, 11408.

(29) Nie, A.; Cheng, Y.; Ning, S.; Foroozan, T.; Yasaei, P.; Li, W.; Song, B.; Yuan, Y.; Chen, L.; Salehi-Khojin, A.; et al. Selective Ionic Transport Pathways in Phosphorene. *Nano Lett.* **2016**, *16*, 2240−2247.

(30) Wen, Q.; Yan, D.; Liu, F.; Wang, M.; Ling, Y.; Wang, P.; Kluth, P.; Schauries, D.; Trautmann, C.; Apel, P.; et al. Highly Selective Ionic Transport through Subnanometer Pores in Polymer Films. *Adv. Funct. Mater.* **2016**, *26*, 5796−5803.

(31) Krems, M.; Pershin, Y. V.; Di Ventra, M. Ionic Memcapacitive Effects in Nanopores. *Nano Lett.* **2010**, *10*, 2674−2678.

(32) Wang, D.; Kvetny, M.; Liu, J.; Brown, W.; Li, Y.; Wang, G. Transmembrane Potential across Single Conical Nanopores and Resulting Memristive and Memcapacitive Ion Transport. *J. Am. Chem. Soc.* **2012**, *134*, 3651−3654.

(33) Wang, D.; Wang, G. Dynamics of Ion Transport and Electric Double Layer in Single Conical Nanopores. *J. Electroanal. Chem.* **2016**, *779*, 39−46.

(34) Woermann, D. Electrochemical Transport Properties of a Cone-Shaped Nanopore: High and Low Electrical Conductivity States Depending on the Sign of an Applied Electrical Potential Difference. *Phys. Chem. Chem. Phys.* **2003**, *5*, 1853−1858.

(35) Woermann, D. Electrochemical Transport Properties of a Cone-Shaped Nanopore: Revisited. *Phys. Chem. Chem. Phys.* **2004**, *6*, 3130−3132.

(36) Cervera, J.; Schiedt, B.; Ramírez, P. A Poisson/Nernst-Planck Model for Ionic Transport through Synthetic Conical Nanopores. *Europhys. Lett.* **2005**, *71*, 35−41.

(37) Kovarik, M. L.; Zhou, K.; Jacobson, S. C. Effect of Conical Nanopore Diameter on Ion Current Rectification. *J. Phys. Chem. B* **2009**, *113*, 15960−15966.

(38) Apel, P. Y.; Blonskaya, I. V.; Orelovitch, O. L.; Ramirez, P.; Sartowska, B. A. Effect of Nanopore Geometry on Ion Current Rectification. *Nanotechnology* **2011**, *22*, 175302.

(39) Kosińska, I. D.; Goychuk, I.; Kostur, M.; Schmid, G.; Hänggi, P. Rectification in Synthetic Conical Nanopores: A One-Dimensional Poisson-Nernst-Planck Model. *Phys. Rev. E* **2008**, *77*, 031131.

(40) Pietschmann, J.-F.; Wolfram, M.-T.; Burger, M.; Trautmann, C.; Nguyen, G.; Pevarnik, M.; Bayer, V.; Siwy, Z. Rectification Properties of Conically Shaped Nanopores: Consequences of Miniaturization. *Phys. Chem. Chem. Phys.* **2013**, *15*, 16917−16926.

(41) Constantin, D.; Siwy, Z. S. Poisson-Nernst-Planck Model of Ion Current Rectification through a Nanofluidic Diode. *Phys. Rev. E* **2007**, *76*, 041202.

(42) Qian, S.; Joo, S. W.; Ai, Y.; Cheney, M. A.; Hou, W. Effect of Linear Surface-Charge Non-Uniformities on the Electrokinetic Ionic-

https://dx.doi.org/10.1021/acs.jpcc.9b10201
J. Phys. Chem. C 2020, 124, 5817−5828

Current Rectification in Conical Nanopores. *J. Colloid Interface Sci.* **2009**, *329*, 376−383.
(43) Plett, T.; Shi, W.; Zeng, Y.; Mann, W.; Vlassiouk, I.; Baker, L. A.; Siwy, Z. S. Rectification of Nanopores in Aprotic Solvents − Transport Properties of Nanopores with Surface Dipoles. *Nanoscale* **2015**, *7*, 19080−19091.
(44) Freemantle, M. *An Introduction to Ionic Liquids*; The Royal Society of Chemistry: London, UK, 2009.
(45) Zeman, J.; Uhlig, F.; Smiatek, J.; Holm, C. A Coarse-Grained Polarizable Force Field for the Ionic Liquid 1-Butyl-3-Methylimidazolium Hexafluorophosphate. *J. Phys.: Condens. Matter* **2017**, *29*, 504004.
(46) Wu, P.; Huang, J.; Meunier, V.; Sumpter, B. G.; Qiao, R. Complex Capacitance Scaling in Ionic Liquids-Filled Nanopores. *ACS Nano* **2011**, *5*, 9044−9051.
(47) Feng, G.; Cummings, P. T. Supercapacitor Capacitance Exhibits Oscillatory Behavior as a Function of Nanopore Size. *J. Phys. Chem. Lett.* **2011**, *2*, 2859−2864.
(48) Perkin, S. Ionic Liquids in Confined Geometries. *Phys. Chem. Chem. Phys.* **2012**, *14*, 5052−5062.
(49) Hayes, R.; Warr, G. G.; Atkin, R. Structure and Nanostructure in Ionic Liquids. *Chem. Rev.* **2015**, *115*, 6357−6426.
(50) Xu, S.; Xing, S.; Pei, S.-S.; Ivaništšev, V.; Lynden-Bell, R.; Baldelli, S. Molecular Response of 1-Butyl-3-Methylimidazolium Dicyanamide Ionic Liquid at the Graphene Electrode Interface Investigated by Sum Frequency Generation Spectroscopy and Molecular Dynamics Simulations. *J. Phys. Chem. C* **2015**, *119*, 26009−26019.
(51) Fedorov, M. V.; Kornyshev, A. A. Towards Understanding the Structure and Capacitance of Electrical Double Layer in Ionic Liquids. *Electrochim. Acta* **2008**, *53*, 6835−6840.
(52) Bazant, M. Z.; Storey, B. D.; Kornyshev, A. A. Double Layer in Ionic Liquids: Overscreening versus Crowding. *Phys. Rev. Lett.* **2011**, *106*, 046102.
(53) Singh, R.; Monk, J.; Hung, F. R. A Computational Study of the Behavior of the Ionic Liquid [BMIM+] [PF6-] Confined Inside Multiwalled Carbon Nanotubes. *J. Phys. Chem. C* **2010**, *114*, 15478−15485.
(54) Singh, R.; Monk, J.; Hung, F. R. Heterogeneity in the Dynamics of the Ionic Liquid [BMIM+] [PF6−] Confined in a Slit Nanopore. *J. Phys. Chem. C* **2011**, *115*, 16544−16554.
(55) Rajput, N. N.; Monk, J.; Hung, F. R. Structure and Dynamics of an Ionic Liquid Confined Inside a Charged Slit Graphitic Nanopore. *J. Phys. Chem. C* **2012**, *116*, 14504−14513.
(56) Rajput, N. N.; Monk, J.; Singh, R.; Hung, F. R. On the Influence of Pore Size and Pore Loading on Structural and Dynamical Heterogeneities of an Ionic Liquid Confined in a Slit Nanopore. *J. Phys. Chem. C* **2012**, *116*, 5169−5181.
(57) Singh, R.; Rajput, N. N.; He, X.; Monk, J.; Hung, F. R. Molecular Dynamics Simulations of the Ionic Liquid [EMIM+] [TFMSI-] Confined inside Rutile (110) Slit Nanopores. *Phys. Chem. Chem. Phys.* **2013**, *15*, 16090−16103.
(58) Wang, Y.; Huo, F.; He, H.; Zhang, S. The Confined [Bmim] [BF4] Ionic Liquid Flow through Graphene Oxide Nanochannels: A Molecular Dynamics Study. *Phys. Chem. Chem. Phys.* **2018**, *20*, 17773−17780.
(59) Wang, Y.; Wang, C.; Zhang, Y.; Huo, F.; He, H.; Zhang, S. Molecular Insights into the Regulatable Interfacial Property and Flow Behavior of Confined Ionic Liquids in Graphene Nanochannels. *Small* **2019**, *15*, 1804508.
(60) Jiang, X.; Qiao, R. Electrokinetic Transport in Room-Temperature Ionic Liquids: Amplification by Short-Wavelength Hydrodynamics. *J. Phys. Chem. C* **2012**, *116*, 1133−1138.
(61) Jiang, X.; Huang, J.; Sumpter, B. G.; Qiao, R. Electro-Induced Dewetting and Concomitant Ionic Current Avalanche in Nanopores. *J. Phys. Chem. Lett.* **2013**, *4*, 3120−3126.
(62) Jiang, X.; Huang, J.; Zhao, H.; Sumpter, B. G.; Qiao, R. Dynamics of Electrical Double Layer Formation in Room-Temperature Ionic Liquids under Constant-Current Charging Conditions. *J. Phys.: Condens. Matter* **2014**, *26*, 284109.
(63) Davenport, M.; Rodriguez, A.; Shea, K. J.; Siwy, Z. S. Squeezing Ionic Liquids through Nanopores. *Nano Lett.* **2009**, *9*, 2125−2128.
(64) Jiang, X.; Liu, Y.; Qiao, R. Current Rectification for Transport of Room-Temperature Ionic Liquids through Conical Nanopores. *J. Phys. Chem. C* **2016**, *120*, 4629−4637.
(65) Jiang, H.; Lee, P. S.; Li, C. 3D Carbon Based Nanostructures for Advanced Supercapacitors. *Energy Environ. Sci.* **2013**, *6*, 41−53.
(66) Humphrey, W.; Dalke, A.; Schulten, K. VMD − Visual Molecular Dynamics. *J. Mol. Graphics* **1996**, *14*, 33−38.
(67) Stone, J. An Efficient Library for Parallel Ray Tracing and Animation. M.Sc. Thesis, Computer Science Department, University of Missouri-Rolla, 1998.
(68) Abraham, M. J.; Murtola, T.; Schulz, R.; Páll, S.; Smith, J. C.; Hess, B.; Lindahl, E. GROMACS: High Performance Molecular Simulations through Multi-Level Parallelism from Laptops to Supercomputers. *SoftwareX* **2015**, *1−2*, 19−25.
(69) Roy, D.; Maroncelli, M. An Improved Four-Site Ionic Liquid Model. *J. Phys. Chem. B* **2010**, *114*, 12629−12631.
(70) Alexiadis, A.; Kassinos, S. Molecular Simulation of Water in Carbon Nanotubes. *Chem. Rev.* **2008**, *108*, 5014−5034.
(71) Hess, B.; Bekker, H.; Berendsen, H. J. C.; Fraaije, J. G. E. M. LINCS: A Linear Constraint Solver for Molecular Simulations. *J. Comput. Chem.* **1997**, *18*, 1463−1472.
(72) Aksimentiev, A.; Schulten, K. Imaging α-Hemolysin with Molecular Dynamics: Ionic Conductance, Osmotic Permeability, and the Electrostatic Potential Map. *Biophys. J.* **2005**, *88*, 3745−3761.
(73) Roux, B. The Membrane Potential and its Representation by a Constant Electric Field in Computer Simulations. *Biophys. J.* **2008**, *95*, 4205−4216.
(74) Cruz-Chu, E. R.; Aksimentiev, A.; Schulten, K. Ionic Current Rectification through Silica Nanopores. *J. Phys. Chem. C* **2009**, *113*, 1850−1862.
(75) Gumbart, J.; Khalili-Araghi, F.; Sotomayor, M.; Roux, B. Constant Electric Field Simulations of the Membrane Potential Illustrated with Simple Systems. *Biochim. Biophys. Acta, Biomembr.* **2012**, *1818*, 294−302.
(76) Nagashima, G.; Levine, E. V.; Hoogerheide, D. P.; Burns, M. M.; Golovchenko, J. A. Superheating and Homogeneous Single Bubble Nucleation in a Solid-State Nanopore. *Phys. Rev. Lett.* **2014**, *113*, 024506.
(77) Tinti, A.; Giacomello, A.; Grosu, Y.; Casciola, C. M. Intrusion and Extrusion of Water in Hydrophobic Nanopores. *Proc. Natl. Acad. Sci. U. S. A.* **2017**, *114*, E10266−E10273.
(78) Liu, J.; Wang, D.; Kvetny, M.; Brown, W.; Li, Y.; Wang, G. Quantification of Steady-State Ion Transport through Single Conical Nanopores and a Nonuniform Distribution of Surface Charges. *Langmuir* **2013**, *29*, 8743−8752.
(79) Yang, L.; Fishbine, B. H.; Migliori, A.; Pratt, L. R. Molecular Simulation of Electric Double-Layer Capacitors Based on Carbon Nanotube Forests. *J. Am. Chem. Soc.* **2009**, *131*, 12373−12376.
(80) Fedorov, M. V.; Kornyshev, A. A. Ionic Liquid Near a Charged Wall: Structure and Capacitance of Electrical Double Layer. *J. Phys. Chem. B* **2008**, *112*, 11868−11872.

https://dx.doi.org/10.1021/acs.jpcc.9b10201
J. Phys. Chem. C 2020, 124, 5817−5828